Arch. Metall. Mater. **70** (2025), 1, 105-117

DOI: https://doi.org/10.24425/amm.2025.152524

B. VENKATESH[1*], C. ANIL KUMAR REDDY[1], M.S.K. DEEPAK[2], MANISH ROY[2]

COMPARISON OF VARIOUS NITRIDING PROCESS OF M 50 NiL STEEL

M 50 NiL steel is a variety of tool steel having high toughness. This steel is potential materials for several bearings of aero-engine. This steel is used in carburized condition. However, nitriding has several advantages over carburizing. The main goal of this work is to compare and contrast the microstructural features, mechanical properties and tribolgical performances of this steel nitrided by gas, liquid and plasma nitriding processes. In view of the above, M 50 NiL steel was nitrided by the processes mentioned above. Microstructural characteristics, mechanical properties, sliding wear response in unidirectional and reciprocation mode were evaluated. The results reveal formation of compound layer in gas and plasma nitrided samples. Surface hardness was comparable for all three nitrided layers. Liquid nitrided specimen indicates best wear resistance in unidirectional and reciprocating sliding conditions. The friction coefficient is lower and wear rate is higher under reciprocating sliding than under unidirectional sliding. While delamination cracks are the main features of unidirectional sliding, cracks perpendicular to the surface were noted under reciprocating sliding.

Keywords: Wear; plasma nitriding; liquid nitriding; gas nitriding; SEM

1. Introduction

Rapid development of science and technology of aerospace engineering resulted in development of materials which can operate in demanding environment. M50NiL steel is a case hardened steel which can resist high-load and high-speed and can retain its hardness up to certain temperatures [1]. This steel has high Ni and low carbon content and this gives rise to increased toughness accompanied by lower hardness. This fact prevents using M 50 NiL steel in heat treated condition and makes it mandatory to use in the surface hardened condition achieved by diffusion treatment. The modification of surfaces of M50 NiL by diffusion treatment can lead to a large residual compressive stress on the surface and this can suppress the nucleation and arrest the propagation of cracks. Diffusion treated M 50 Nil steel is suitable for the application to advanced turbine where bearing material requires surviving 100 billion circle under rolling contact. Although several types of coatings are applied for bearing components such as PVD, CVD etc. [2-7] research on diffusion coatings such as gas carburizing [8], nitriding [9], plasma carburizing [10] and nitrocarburizing [11,12] on M50NiL is more promising.

As mentioned above, there exists different diffusion coating processes that can be applied to M 50 NiL steel [13]. Although M 50 NiL steel is routinely used in carburized condition, nitride M 50 Nil can be considered to have more potential. Nitriding by high energy beam such as laser etc. can be more promising. However, due to cost, process control and surface finish, gas nitriding can be seen as more practical for application. Nitriding is one such process with associated advantages of formation of relatively inert layer, introduction of residual compressive stresses, processing at relatively lower temperature etc. There are several nitriding processes such as gas nitriding, liquid nitriding, plasma nitriding etc. Gas nitriding offers advantages of having large batch size, uniform nitriding effect at all corners of the parts, less equipment cost etc. In contrast, liquid nitriding is a fast and simple process. Plasma nitriding which is most popular and commonly practiced in present day ensures enhanced process control, least post nitriding operation, minimum dimensional distortion, clean environment and it is an energy efficient fast process.

Over the years several steels are nitrided using various techniques [14-17]. Even M 50 Nil steel has been nitrided employing liquid and plasma nitriding process [18,19]. The wear

[1] DEPARTMENT OF MECHANICAL ENGINEERING, VARDHAMAN COLLEGE OF ENGINEERING, HYDERABAD-501218, INDIA
[2] DEFENCE METALLURGICAL RESEARCH LABORATORIES, KANCHANBAGH, HYDERABAD-500058, INDIA

* Corresponding author: bvt2275@gmail.com

behaviour of these steels including M 50 Nil is also reported. However, the work on nitriding of M 50 NiL steel is very much limited. A systematic comparison on various nitriding processes and tribological performances of nitided layer of this steel is not available in the literature. Thus, the present work is undertaken to compare and contrast the microstructural characteristics and sliding wear response of M 50 Nil steel nitrided employing various nitriding process such as gas nitriding, liquid nitriding and plasma nitriding. Microstructural constituents of the nitride surface obtained by various processes are highlighted. The material removal mechanisms during unidirectional and reciprocating sliding wear were highlighted and were found to be different.

2. Experimental details

2.1. Gas nitriding

Gas nitriding was carried out by heating the specimen M 50 Nil to a temperature 545°C and holding in ammonia having purity of 99.99% for 90 hrs. This is why the process is sometimes known as ammonia nitriding. The pressure of the nitriding chamber was maintained at 0.01 MPa during the process and the ammonia flow rate was maintained at 200 ml/min. After nitriding the ammonia flow was stopped and the specimens were cooled to ambient temperature in the nitriding furnace. As ammonia dissociates into hydrogen and nitrogen after coming in contact with the specimen, nitrogen starts diffusing onto the metal surface and creates a nitrided layer. Depending on the temperature the solubility of nitrogen into iron varies. Nitriding for long duration ensures increased depth of nitrided layer and complete transformation of carbides. The samples were thoroughly cleaned and degreased prior to nitriding.

2.2. Liquid nitriding

Liquid nitriding was performed in a salt bath containing alkaline cynates and carbonates in 70 : 30 ratio. The samples were degreased with trichloroethylene and cleaned in 5% sulphuric acid followed by rinsing in water and drying prior to nitriding. The specimen was held at 550°C for 3hrs. As the temperature is increased, alkaline cynates dissociates and oxidizes to give nitrogen for nitriding to proceed. Alkaline cynates and carbonates were periodically added to ensure constant source of nitrogen. Salt bath nitriding is much faster process than gas nitriding and depth of nitride layer is determined by time and temperature of the process.

2.3. Plasma nitriding

Plasma nitriding was carried out in a LDMC-30t plasma nitriding unit. The samples were cleaned ultrasonically in acetone and then cleaned in flowing water prior to nitriding. The vacuum in the nitriding chamber was maintained at 5 mbar with the help of a rotary pump prior to development of the glow discharge. The chamber which acts as anode was connected to ground potential. The specimen holder on the other hand was connected to negative potential and this acted as cathode. Plasma nitriding was performed at 520°C for 40 hrs in mixed gases of nitrogen and hydrogen with flow rates of 80 cm^3 and 20 cm^3. The samples were cooled slowly to the room temperature in the chamber in protective of nitrogen atmosphere to eliminate possible oxidation. The schematic representation of the process is made in Fig. 1. The temperature and time of various nitriding procedure are listed in TABLE 1.

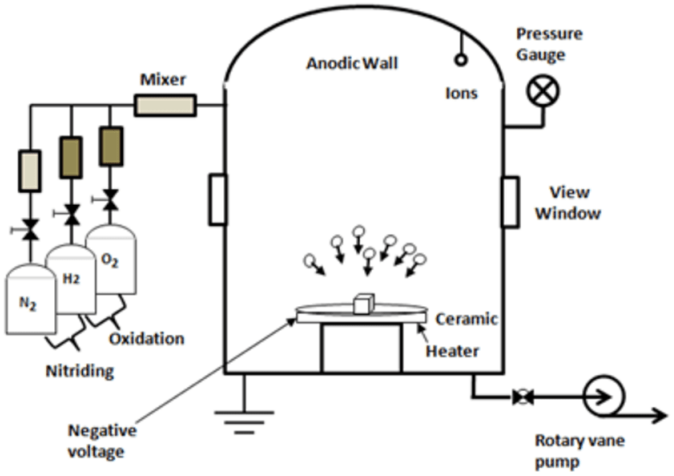

Fig. 1. Schematic representation of plasma nitriding unit

TABLE 1

Time and temperature of various nitriding processes

Nitriding Process	Temperature (K)	Time (s)
Gas nitriding	818	324000
Liquid nitriding	823	10800
Plasma nitriding	793	144000

2.4. Characterisation of nitride layer

X-ray diffraction (XRD) pattern of the nitrided surface was obtained using a Philips PW 1830 diffractometer to examine the structure of the nitrided layer. The setting of the X-ray diffractometer was done at 40 kV and 30 mA with Co K_α radiation target and a nickel filter. The recording of the diffraction patterns was done at a speed of 0.01° s^{-1}. The nitrided samples were then sectioned transversely and transverse sections were examined under optical and scanning electron microscopy (SEM) after metallographically polishing the sectioned surfaces. Microhardness of the nitrided layer was evaluated on the transverse sectioned surfaces employing 'Omnitech' microhardness tester model No F. AUTO at a load of 50 gms with the help of a Knoop indenter. Hardness measurement parameters are summarized in TABLE 2.

TABLE 2

Hardness measurement parameters

Indenter used	Knoop
Applied load (gm)	50
Loading time (s)	10
Holding time (s)	5
Unloading time (s)	10

2.5. Wear testing

Ball on disc configuration was used for wear testing in this work in line with ASTM G-99-10. Tests were done at room temperature at 70% humidity. Tests were performed for loads 20 N, and at sliding speeds of 1.0 m/s under unidirectional test. Under reciprocating test also applied load was 20 N. Friction coefficient was continuously monitored. Repetition of each test was done for three times. The schematic diagram of the rig is presented in Fig. 2. Test was conducted for a sliding distance of 1800 m under unidirectional sliding. The wear test conditions under unidirectional sliding and reciprocating sliding are listed in TABLE 3 and TABLE 4 respectively. Wear volume was measured at the end of the test using non-contact optical profilometer of Taylor Hobson bearing model no CCI MP M112 4424 02. The wear test rig is manufactured by Rtec Instrument having model no MFT 5000. The wear volumes of the disc (W_d) and that of the ball (W_b) were estimated using the equation given below [20]

$$W_d = 2\pi r_w A \tag{1}$$

Where, r_w and A are the radius of the wear track and the cross sectional area of the track respectively.

$$W_b = \frac{\pi h^2 (3R - h)}{3} \tag{2}$$

$$h = R - \sqrt{R^2 - r^2} \tag{3}$$

Where, R, r and h are the radius of the ball, the radius of the wear scar and the height of the worn surface respectively.

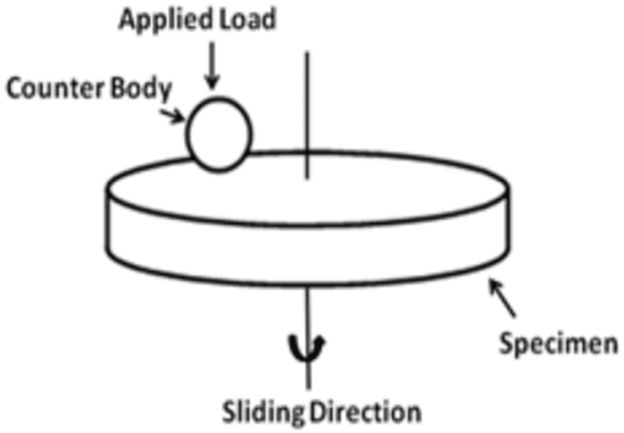

Fig. 2. The schematic diagram of the wear test facility

TABLE 3

Unidirectional sliding wear test condition

Test Configuration	Ball on Disc
Applied Load	20 N
Sliding Speed	1 m/s
Counter body	52100 steel

TABLE 4

Reciprocating sliding wear test condition

Test Configuration	Ball on Disc
Applied Load	20 N
Stroke Length	6 mm
Frequency	10 Hz
Counter body	52100 steel

2.5. Examination of worn surfaces

The worn surfaces were viewed with the help of a SEM having energy dispersive spectrometer (EDS) to assess the chemistry and the morphology of the worn surfaces and to understand the material loss mechanisms. The transverse sections of the worn surfaces were also examined under SEM to substantiate understanding of degradation mechanism.

3. Results and discussion

3.1. Microstructural features

The X-ray diffraction pattern obtained from as received nitride surfaces are presented in Fig. 3. Peak corresponding to cubic γ-Fe_4N and hexagonal ε-$Fe_{2.3}N$ are identified in addition to cubic matrix phases α-Fe and tetragonal α/-Fe (N). Ɛ-$Fe_{2.3}N$ contains broad range of nitrogen from $F_{3.2}N$ (24 at%) to F_2N (33 at%). However, such alteration of nitrogen content gives rise to the maximum 1% volume change. The nature of pattern is more or less similar for all three nitriding processes. However, marginal shifting of peaks can be noted due to strain as a result of the processes. The transverse sections of the nitrided layers are illustrated in Fig. 4. Fig. 4a, 4b and 4c correspond to gas nitrided, liquid nitrided and plasma nitrided sections. A weak contrast between the core and the nitrided layer is to be noted. Both samples nitrided by gas and liquid nitriding techniques exhibit the presence of 4-5 μm thick continuous white layer. In contrast, no white layer can be noted on the surfaces of plasma nitrided sample. It however, shows the presence of pores near the surface region. The presence of such white layer is noted in M 50 Nil and other steel nitrided by plasma nitriding technique [21-23]. As one goes further interior from the surface, ferritic layer saturated with interstitials can be noted as evident from XRD pattern for all three nitrided samples. Since diffraction pattern exhibits presence of γ-Fe_4N and ε-$Fe_{2.3}N$, the white layer consists of both the phases. As noted in previous investigations,

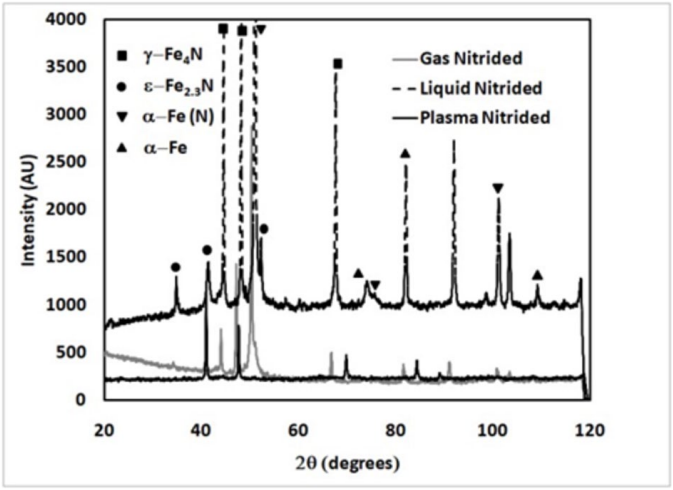

Fig. 3. XRD pattern from various nitride surfaces

ε-$Fe_{2.3}N$ is harder and more brittle than γ-Fe_4N [24]. Thus, higher content of γ-Fe_4N in the white layer is desirable. A network of white precipitates can be noticed throughout the nitrided layer after gas nitriding. These precipitates are expected to be γ-Fe_4N [25]. Long duration of gas nitriding helps in transforming carbides to nitrides. The released carbon will diffuse to the diffusion front of nitrogen and form cementite precipitate along the grain boundary [26,27]. Some amount of carbon will be escaped from the surface giving rise to decarburization and this condition is favorable for the formation of γ-Fe_4N [28]. The diffusion zone of gas nitrided layer can further be divided into two different sub layers namely sub layer containing carbides transformed to nitrides and sub layer containing untransformed carbides. The liquid nitrided sample exhibits presence of multilayer as noted by other investigators [29-31]. Although, maximum number of peaks can be seen in liquid nitrided condition, peaks corresponding to similar phases can be seen in other nitrided conditions as well. Small shifting of peaks and broadening of peaks can be seen. This is due to residual stresses, nitrogen content or size of lattice parameter and defect structures of nitrided layers [32]. The presence of S phases [33], CrN phase or other oxide phases as noted by other on the surface of salt bath nitrided layer [34,35] was not detected. Inside the α-Fe (N) layer, Fe_4N are dispersed uniformly. Plasma nitriding of steel including that of M 50 Nil steel [18,19] has been carried out by several investigators [36-38]. γ-Fe_4N and ε-$Fe_{2.3}N$ phases were identified in plasma nitrided samples of steels [37,38] including M 50 NiL steel [19]. It is to be stated that, if plasma nitriding is carried out at lower temperature, γ-Fe_4N phase does not form [39]. The thickness of nitrided layers observed under microscopy is presented in Fig. 5. Clearly the thickness of plasma nitrided layer is significantly higher than layers obtained by other two nitriding processes. The presence of white layer is reported for gas nitrided H13 steel by Berraiset al. [40] and gray cast iron by Zheng et al. [41]. A comparable thickness of nitrided layer of a gas nitrided high carbon high chromium steel was reported by Duan et al. [42]. Although the thickness of nitrided layer was comparable to the present work, the thickness of the compound layer was significantly less. They however, carried out the nitriding for a significantly less time. A thickness of 100 μm nitrided layer for H13 steel is obtained by Castro et al. [43] at 580°C for 3 hrs and around 50 to 62 μm with 316 LN SS by Murali et al. [44] at 560°C for 1 to 2 hrs. through sursulf process. This thickness is in line with present work. However, they have not seen compound layer when nitrided for less than 7 hrs. In contrast, Peng et al. [45],

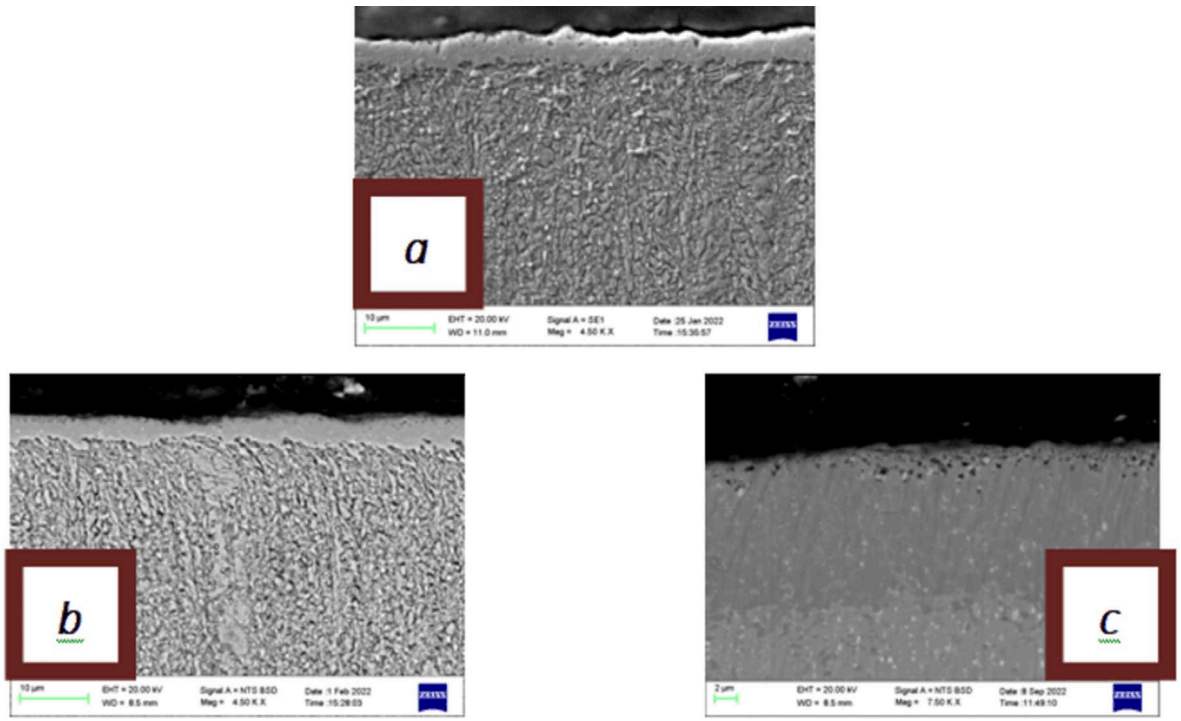

Fig. 4. SEM images of the microstructures of a) Gas nitrided at 545°C for 90 hrs. b) liquid nitrided at 550°C for 3 hrs. and c) plasma nitrided at 520°C for 40 hrs

Shih et al. [46] Wang et al. [33] observed presence of compound layer and the thickness of compound layer was around 4 µm when nitrided in salt bath at 530°C for an hour with AISI 1045 steel and 3 µm when nitrided at 650°C for 2 hrs. with 304 SS. The thickness of their nitrided layer was also close to 100 µm when nitrided for 2 hrs. The presence of compound layer during plasma nitriding of steel is confirmed by Valdes et al. [47], Chen et al. [48], Yang et al. [49], Jacobsen et al. [23], Zagonel et al. [50], Soleimani et al. [51], Fernandes et al. [52] and Karamış et al. [53]. Thickness of plasma nitride compound layer was found to be 1 to 3 µm by Chen et al. for 304 SS [48], 3 to 4 µm by Yang et al. [49] for 4140 steel, 4 µm by Jacobsen et al. [23] for H13 steel and 4 to 5 by Karamış et al. [53] for H11 steel. Around 100 µm thick nitrided layer for M 50 steel is obtained by Yao et al. [44] by nitriding at 530°C for 6hrs. Significant lower thickness of plasma nitrided layer is reported by Manfrinato et al. [54]. Jacobsen et al. [23], Zagonel et al. [50]. Jacobsen et al. [21] however, obtained a compound layer of 13 µm thickness and a diffusion layer of in excess of 200 µm thickness by carrying out plasma nitriding under high current density. Soleimani et al. [51] and Fernandes et al. [52] reported thickness of nitrided layer close to 400 µm for H13 steel by plasma nitriding and this thickness is consistent with present work.

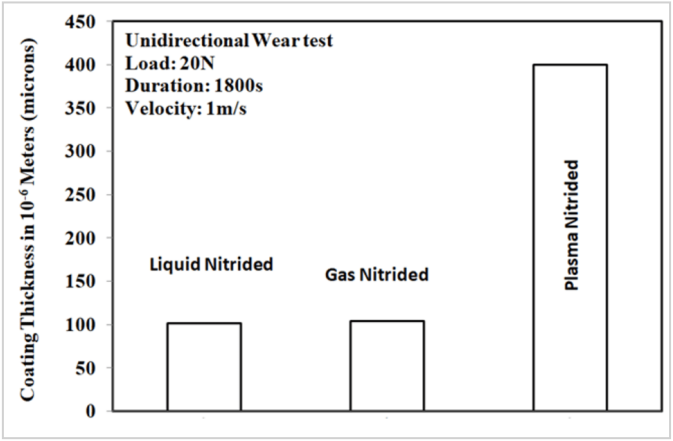

Fig. 5. thickness of various nitride layers

3.2. Mechanical properties of the nitride layers

The bar diagram showing the surface hardness of all three nitrided layers are given in Fig. 6. The hardness is around 800 HV for liquid and gas nitride samples. The plasma nitrided sample exhibits marginally higher value. Comparable surface hardness was reported by Duan et al. [42] for high carbon high chromium steel, Zheng et al. [41] for grey cast iron processed through gas nitriding. The surface hardness of 1100 HV were obtained for gas nitrided additively manufactured maraging steel by Funch et al. [55], H13 steel by Berrais et al. [40]. Similarly comparable hardness was obtained with the help of salt bath nitriding of chrome moly steel by Chen et al. [17], of 1045 steel by Peng et al. [45]. Higher hardness close to 1100 HV is noted by Castro et al. [43] for H13 steel, by Luo et al. [56] for 316L steel nitride through liquid nitriding. A hardness of 1400 HV is reported by Wang et al. [33] for 321 stainless steel, Murali et al. [44] for 316 LN stainless steel, nitrided using salt bath nitriding technique. A hardness between 800 to 1000 has been attained through various plasma nitriding of 1045 steel by Naeem et al. [16], maraging steel by Godec et al. [56], AISI 321 steel by Manfrinato et al. [54], 4140 steel by Yang et al. [49], H13 steel by Jacobsen et al. [23], H13 steel by Fernandes et al. [52] and H11 steel by Karamış et al. [53]. Hardness in excess of 1200 HV through plasma nitriding is noted by Yao et al. [22] for M 50 steel, Zagonel et al. [50] for H13 steel. Significantly lower hardness around 500 HV is reported by Soleimani et al. [51] for plasma nitrided cold work tool steel. The hardness profiles showing the variation of hardness with the depth of nitrided layer is provided in Fig. 7. The thickness of nitrided layer as evident from the profile is around 150 µm for gas and liquid nitrided samples. It is significantly higher and is around 450 µm for plasma nitrided sample. This observation is in line with that observed under electron microscopy. It is also to be stated that the hardness monotonically decreased from the highest value on the surface to beneath the surface in the present work and such response is noted for

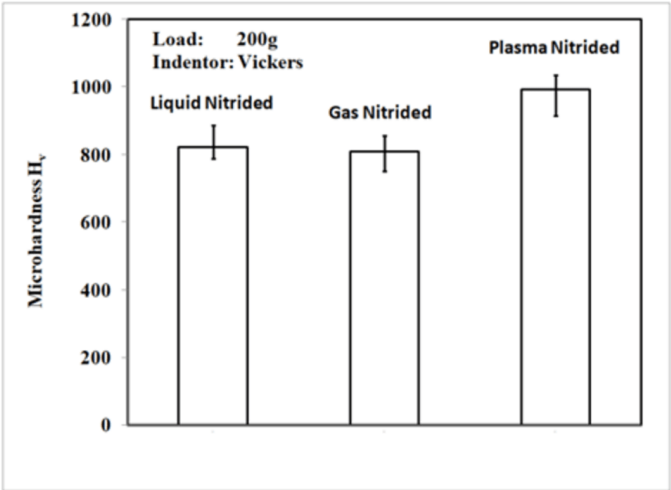

Fig. 6. Hardness of various nitride surfaces

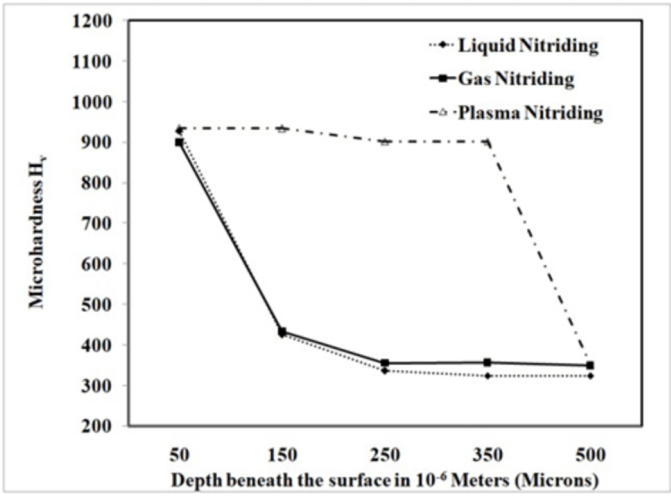

Fig. 7. Hardness profiles across the nitride layers

all three types of nitriding process namely, gas nitriding, liquid nitriding and plasma nitriding. Available literature on gas nitriding [40-42,55] and salt bath nitriding indicates the trend similar to present work. Most investigators observed similar trends in measurement of hardness profiles [16,21,22,49,50,54,56] even in case for plasma nitriding. However, few investigators observed the maximum hardness few microns below the surface [52,53]. Others observed both monotonaically decreasing hardness and the maximum hardness at intermediate region [23,51]. The reason for this type of response can be attributed to the fact that most processes which exhibited the maximum hardness at an intermediate region were carried out for long duration and the surface contained lower amount of ε-$Fe_{2.3}N$ phase than γ-Fe_4N phase. A soft γ-Fe_4N phase results in lower hardness on the surface. It is also possible due to the formation of oxide scale having lower hardness than both the ε-$Fe_{2.3}N$ and γ-Fe_4N phases, on the surface. Plasma nitrided layer did not show the presence of any white layer. Thus, the nitride layer is containing various amounts of cubic γ-Fe_4N, cubic α-Fe and tetragonal $\alpha^{/}$-Fe (N) in such proportion that the hardness of the nitrided layer is nearly constant throughout except near interface.

3.3. Friction response

The variation of friction coefficient as function of time under unidirectional sliding condition is shown in Fig. 8. The friction coefficients are around 0.5 to 0.6 and are equal for all three nitrided surfaces. Comparable friction coefficient of various nitrided layers on different substrates was reported previously [21,57]. The friction coefficient of gas nitrided grey cast iron was significantly higher than this value [41]. The friction coefficient of salt bath nitrided H13 steel [43] and 316LN steel [44] are in conformity with present work. Significantly lower friction coefficient was noted for plasma nitrided H13 steel by Leite et al. [15]. However, slightly higher friction coefficient of plasma nitrided layer than present work was obtained by Jecobson et al. [23] for H13 steel, Yang et al. [49] for 4140 steel, Uzun [14] for 316L steel. Work due to Yao et al. [22] and Wang et al. [33] indicated friction coefficient comparable to the present study for M 50 and M 50 NiL steel respectively nitrided by plasma technique. Naeem et al. [16] reported friction coefficient lower, comparable and higher than this work depending on plasma nitriding conditions for 1045 steel. Similarly the variations of friction coefficient as function of sliding time under reciprocating sliding condition for all three nitride layers are given in Fig. 9. Under reciprocating sliding condition, friction coefficient is significantly lower than that under unidirectional sliding. Fiction coefficient is around 0.1 for gas and plasma nitrided sample. It is slightly higher around 0.15 for liquid nitrided sample. These values are substantially lower than that obtained by Duan et al. [42] during fretting wear of gas nitrided high carbon high chromium steel, by Godec et al. [56] during reciprocating wear of plasma nitrided additively manufactured maraging steel.

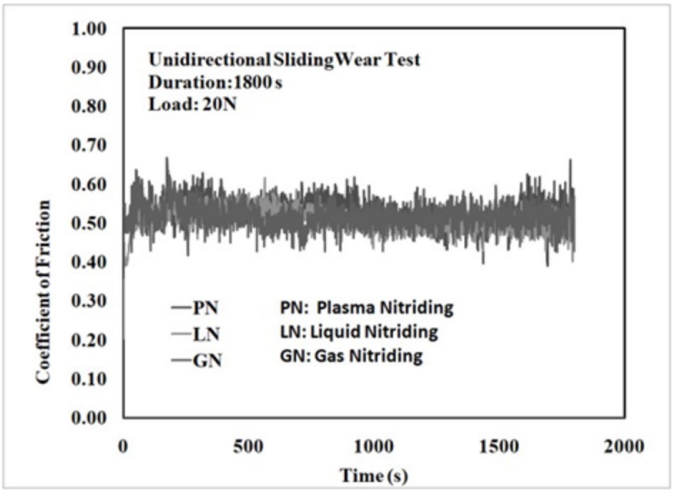

Fig. 8. Variation of friction coefficient of various nitride layers as function of sliding time under unidirectional sliding

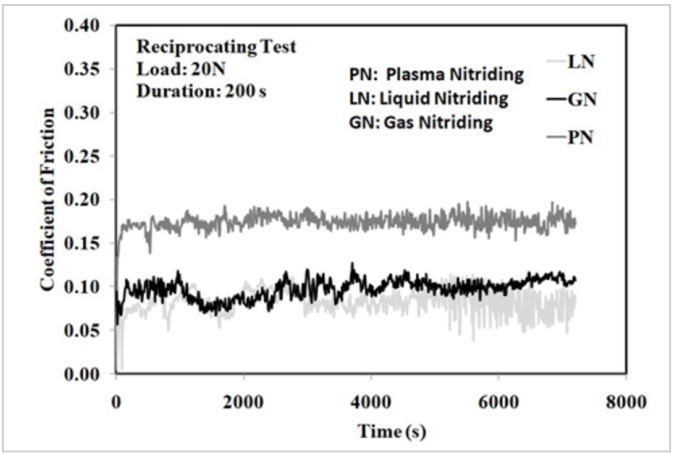

Fig. 9. Variation of friction coefficient of various nitride layers as function of sliding time under reciprocating sliding

3.4. Wear behaviour

The bar diagram showing the wear depth under unidirectional sliding of various nitrided layers is presented in Fig. 10. It is clear from Fig. 10 that the highest wear depth corresponds to gas nitrided layers. In contrast, the least wear depth pertains to liquid nitrided layer. The plasma nitrided layer exhibits intermediate wear depth under unidirectional sliding. The wear depth of gas nitrided layer is nearly 3 times the wear depth of liquid nitrided layer under unidirectional sliding. The bar diagram showing wear depth under reciprocating sliding is shown in Fig. 11. The wear depth is higher during reciprocating wear than that during unidirectional sliding for specimens nitrided under similar condition. Under reciprocating sliding condition also liquid nitrided layer exhibits the minimum wear depth. The highest wear depth however, is shown by gas nitrided layer under reciprocating sliding also. Plasma nitrided layer is having an intermediate wear depth. Unlike unidirectional wear the wear depth of gas nitrided layer is nearly double the wear depth of liquid nitrided layer under reciprocating sliding.

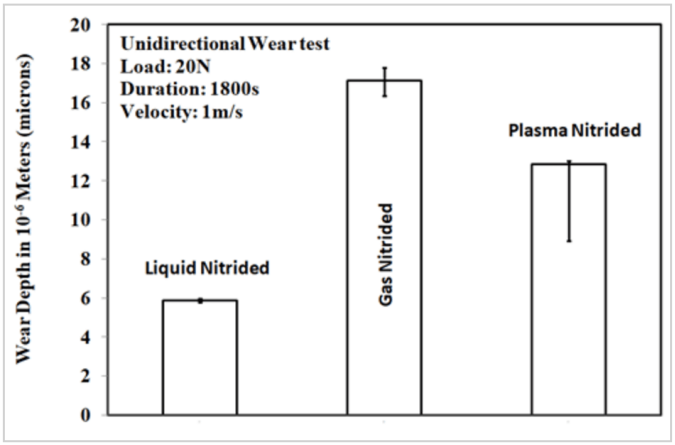

Fig. 10. Bar diagram showing the wear depth of various nitride layers under unidirectional sliding

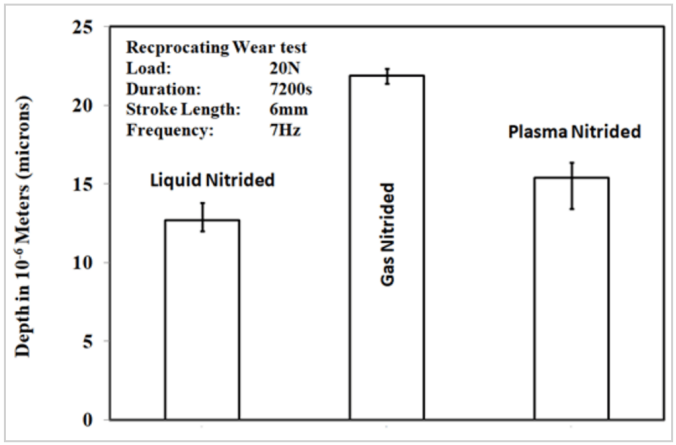

Fig. 11. Bar diagram showing the wear depth of various nitride layers under reciprocating sliding

TABLE 5

Hardness and wear rates of various nitrided layers

Nitriding process	Surface Hardness (HV)	Wear (unidirectional) (mm)	Wear (Reciprocating) (mm)
Gas nitriding	899	17.12	21.86
Liquid nitriding	927	5.95	12.67
Plasma nitriding	334	12.85	15.4

The hardness and wear rates of various nitride layers are provided in TABLE 5. Clearly hardness does not correlate with wear rate. As the unidirectional test was conducted for 1800 m, the specific wear rates under unidirectional condition corresponds to 0.0095, 0.0033 and 0,0071 µm/m for gas, liquid and plasma nitrided samples respectively.

3.5. Characterisation of worn surfaces

The low magnification SEM images of the surfaces, worn at 20 N load under unidirectional sliding of liquid nitrided, gas nitrided and plasma nitrided samples are presented in Fig. 12. The presence of wear debris can be seen on all worn surfaces. Features of plastic deformation are visible on the worn surface of liquid and gas nitrided samples. In contrast, plasma nitrided worn surface is relatively featureless. High magnification micrographs of liquid, gas and plasma nitrided worn surfaces are illustrated in Fig. 13. Gas nitrided surface exhibits transfer of materials from counter-body indicating adhesion dominated wear mechanism. Delamination wear and the presence of surface cracks are predominant features of liquid nitrided surface. Finally, parallel ridges can be seen on the worn surface of plasma nitrided surface.

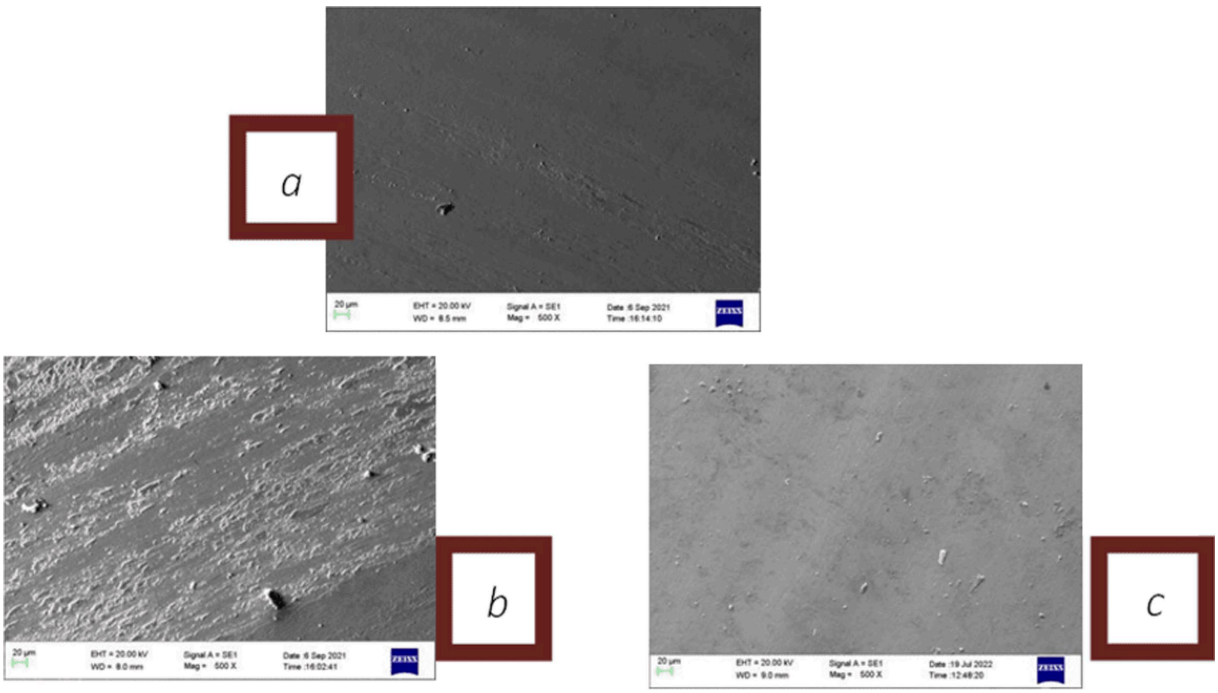

Fig. 12. Low magnification SEM images of the surfaces worn under unidirectional sliding at 20 N applied load, a) gas nitrided for 90 hrs., b) liquid nitrided at 550°C for 3 hrs., c) plasma nitrided at 520°C for 40 hrs

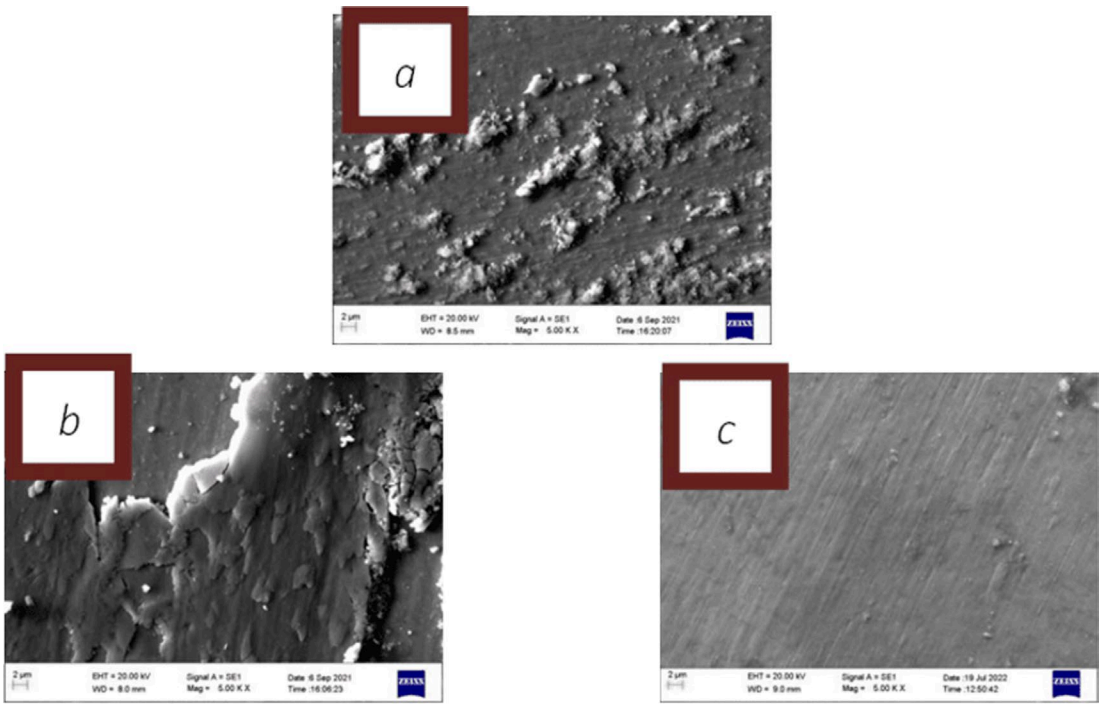

Fig. 13. High magnification SEM images of the surfaces worn under unidirectional sliding at 20 N applied load, a) gas nitrided for 90 hrs. b) liquid nitride for 3 hrs., c) plasma nitrided at 520°C for 40 hrs

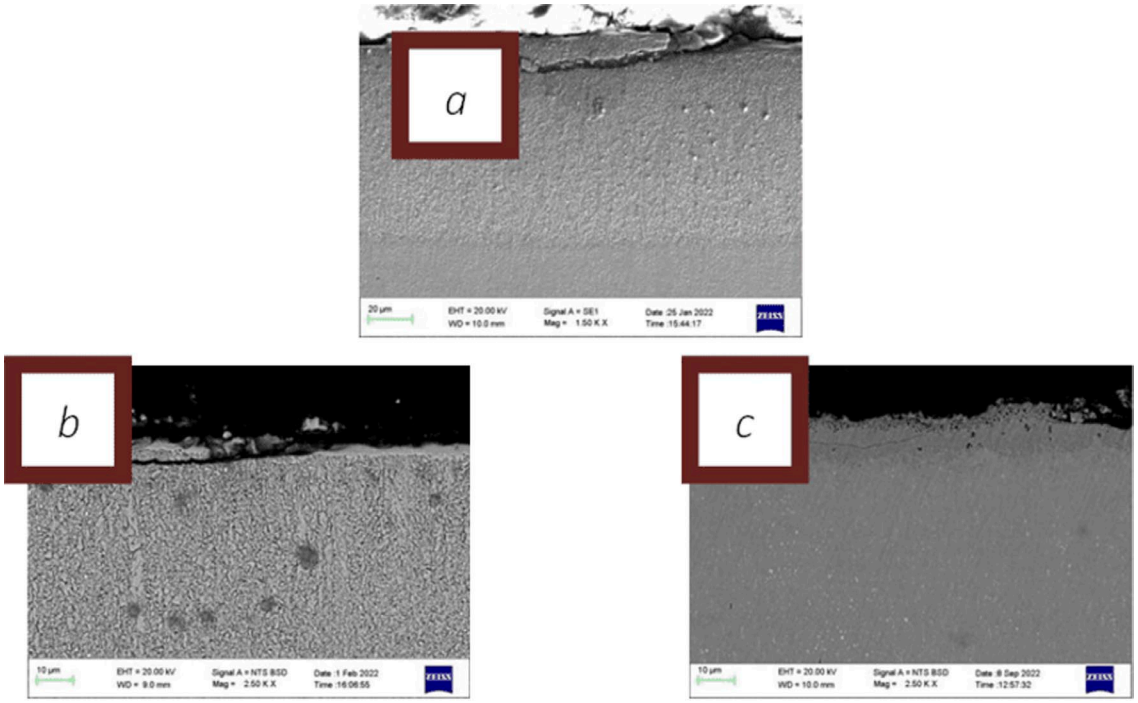

Fig. 14. Transverse section of nitride samples worn under unidirectional sliding at 20 N applied load, a) gas nitrided for 90 hrs. b) liquid nitride for 3 hrs., c) plasma nitrided at 520°C for 40 hrs

This indicates abrasion in addition to adhesion contributes to the wear of plasma nitrided layer. Transverse sections of worn surfaces are shown in Fig. 14. Transverse section of gas nitrided layer shows complete removal of white layer and delamination cracks parallel to the surface. Similar features characterised by delamination crack can be noted on the surfaces beneath the worn surface of liquid nitrided and plasma nitrided surface. However, white layer is found to be adherent to the diffusion layer in liquid nitrided surfaces. This white layer being very hard is wear resistant and leads to decreased wear rate. In contrast, the poor adhesion of white layer to the diffusion layer gives rise to increased wear rate of gas nitrided layer. Further, exposed diffusion layer is susceptible to adhesion of transfer layer from counter-body as noted in Fig. 13b. Adherent white layer was

also obtained by surf sulf process by Krishnaraj et al. [58]. Of course no white layer was noted for plasma nitrided surfaces. The plasma nitrided surface has high hardness and slowly wears out by delamination wear. Because of high depth of hard layer, adhesion of materials from the counter-body was negligible. Further diffusion layer allowed entrapment of debris between the plasma nitrided layer and the counter-body giving rise to abrasive wear. These reasons are responsible for intermediate wear rate of plasma nitrided surface. Similar entrapment of hard debris on nitrided surfaces is reported by Karamis et al. [53], Castro et al. [43], Murali et al. [44] and Naeem et al. [16]. Adhesion and abrasion controlled wear mechanism is also observed

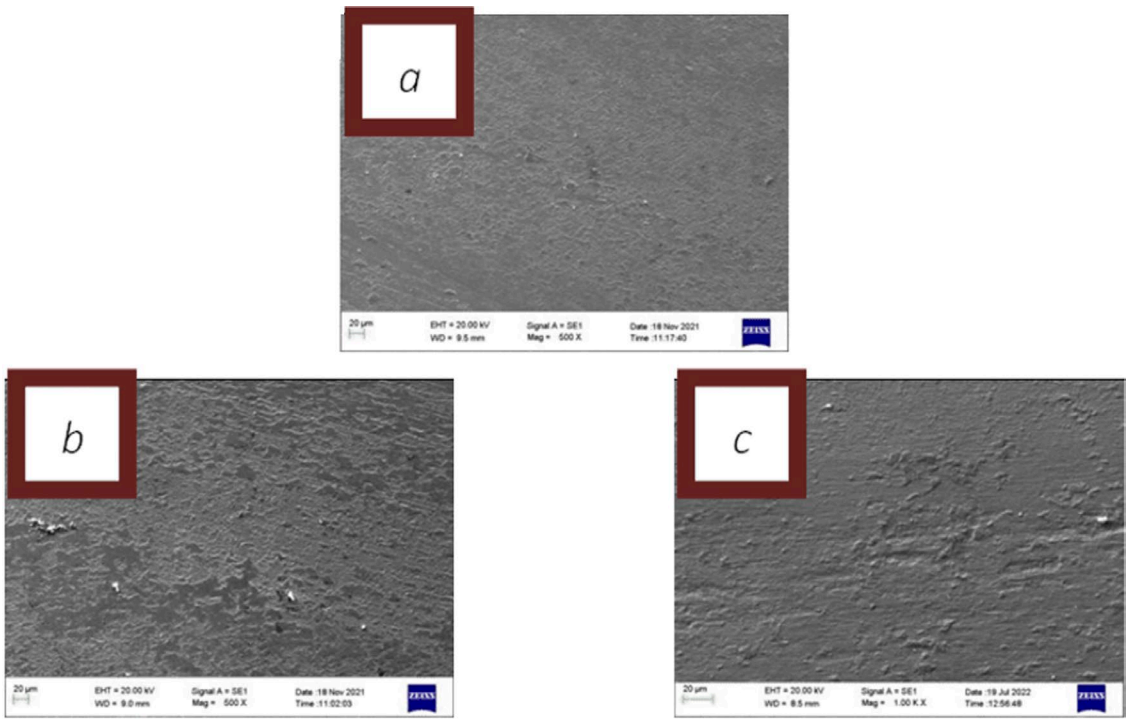

Fig. 15. Low magnification SEM images of the surfaces worn under reciprocating sliding at 20 N applied load, a) gas nitrided for 90 hrs., b) liquid nitride for 3 hrs., c) plasma nitrided at 520°C for 40 hrs

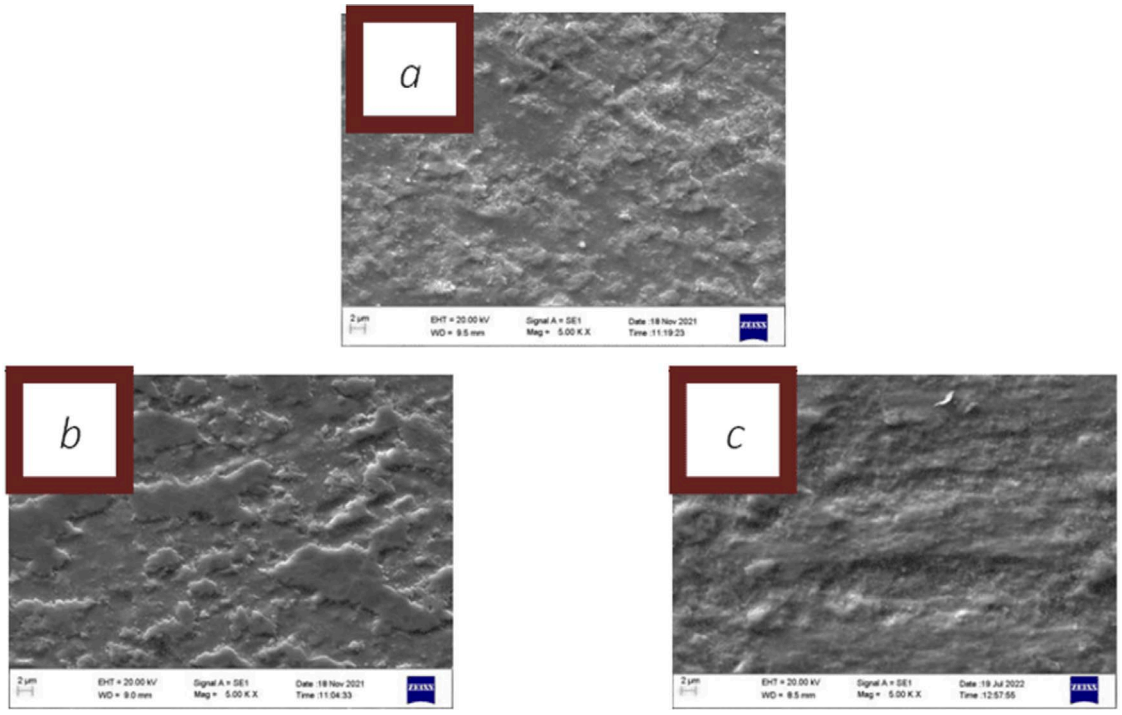

Fig. 16. High magnification SEM images of the surfaces worn under reciprocating sliding at 20 N applied load, a) gas nitrided for 90 hrs., b) liquid nitride for 3 hrs., c) plasma nitrided at 520°C for 40 hrs

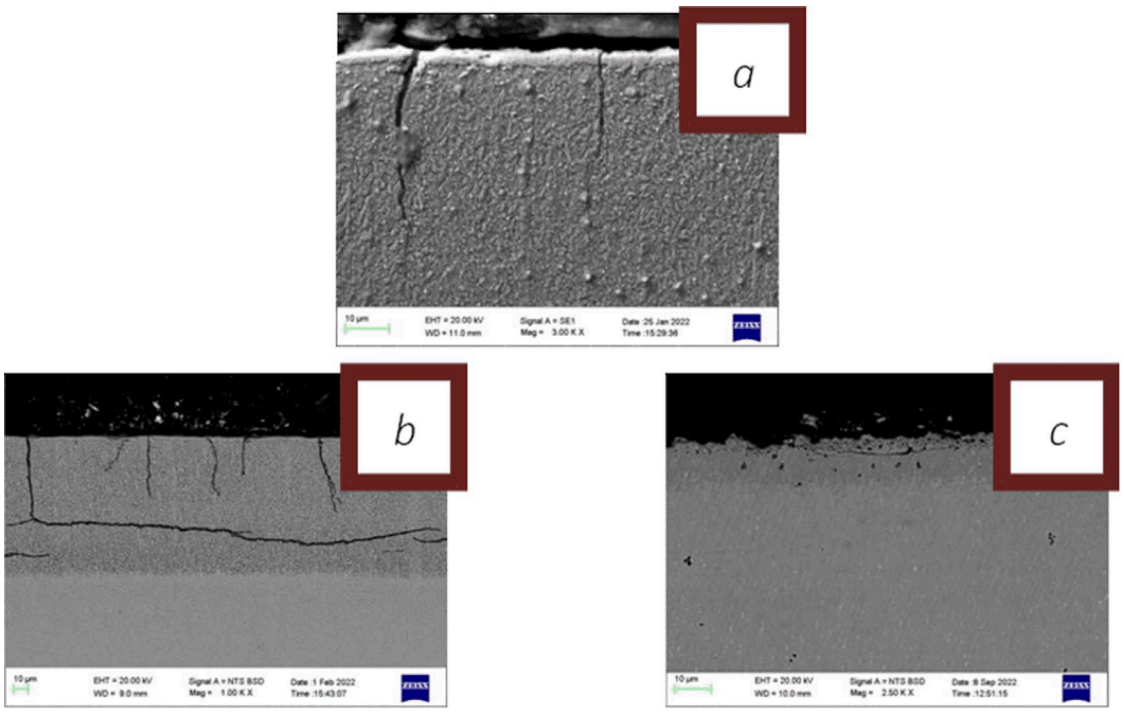

Fig. 17. Transverse section of nitrided samples worn under reciprocating sliding at 20 N applied load, a) gas nitrided for 90 hrs., b) liquid nitride for 3 hrs., c) plasma nitrided at 520°C for 40 hrs

by Yao et al. [22] for M 50 steel plasma nitrided at low and high temperature respectively.

Low magnification micrographs of nitrided surfaces worn by reciprocating motion are given in Fig. 15. Generally featureless surfaces with scattered debris can be seen. High magnification micrographs from Fig. 16 indicate highly deformed surfaces. Adhesion again plays important role in wear of gas nitrided sample under reciprocating condition. Transverse sections of the worn surfaces are provided in Fig. 17. Vertical cracks originated from the surfaces can be noted. It can also be noted that adhesion of white layer is good for both gas nitrided and liquid nitrided layer and this resulted disappearance of adhesion layer from counter-body on the worn surface of gas nitrided layer. The presence of white layer is also responsible for lower differences of the wear rate between gas nitrided and liquid nitrided layer. Further, the presence of vertical cracks is able to accommodate shear stress giving rise to lower friction coefficient in case of reciprocating wear than unidirectional sliding wear. However, such vertical layers results higher wear rate during reciprocating wear than that during unidirectional sliding wear. Plasma nitrided layer exhibits cracks parallel to the surface as noted in unidirectional sliding. It is interesting to note that cracks parallel to the surface in case of plasma nitrided surface is more prominent beneath the surface in case of unidirectional sliding and more prominent near the surface for reciprocating sliding. It is also to be stated that abrasion marks are not seen on the surfaces worn by reciprocating sliding and this rules out entrapment of debris. The friction coefficient is found to be comparable irrespective of prevailing wear mechanism during unidirectional sliding of various nitrided layers. In contrast, friction coefficient is higher for gas nitrided layer than layers nitrided by liquid nitriding or plasma nitriding process. This confirms that adhesion governs friction coefficient during reciprocating sliding of gas nitrided layers also. At this stage, it is pertinent to mention that features associated with mild oxidation or severe oxidation wear [59] are not seen on the surfaces worn either by unidirectional sliding or reciprocating sliding. Further various types of transfer layers such as mechanically mixed layer or composite layers etc. as reported earlier [60,61] are also not noted in present investigation.

4. Conclusions

In the present study M 50 NiL steel has been nitrided using gas, liquid and plasma nitriding processes and are subjected to unidirectional sliding wear and reciprocating sliding wear. The main conclusions are:

- Gas nitriding and liquid nitriding results in formation of 4-5 μm thick white layer also known as compound layer. No such layer is formed by plasma nitriding.
- Surface hardness is comparable for all three nitrided layers. However, depth of plasma nitrided layer is significantly higher than that of gas or liquid nitrided layers.
- The friction coefficients under unidirectional sliding are comparable for all three nitrided layers. During reciprocating sliding friction coefficient of gas nitrided layer is higher than that of liquid or plasma nitrided layer. Further, friction coefficient during reciprocating sliding is lower than that of unidirectional sliding for surfaces nitrided under similar conditions.
- The wear rate of gas nitrided layer is the highest under unidirectional or reciprocating sliding. In addition, wear

rate under reciprocating sliding is higher than that under unidirectional sliding for samples nitrided under identical condition. Liquid nitrided layer exhibits the best wear resistance under both type of wear.

- Delamination cracks characterized by the formation of cracks beneath the worn surface and propagation of cracks parallel to the worn surface are the main features of the subsurface of specimen subjected to unidirectional sliding. In contrast, under reciprocating sliding, cracks perpendicular to the worn surface are formed.
- As future outlook, a more comprehensive wear study i.e. nitrided samples are to be subjected to wear under different conditions, should be carried. Wear in presence of corroding environment also constitutes important direction of future study as nitrided layers are more inert than as received surfaces. Finally, examination of laser nitrided layers is also a potential area of future research.

Acknowledgement

This research was funded through the research grants by Aeronautics Research and Development Board (DRDO), New Delhi. The authors gratefully acknowledge the support of ARDB for this paper work.

REFERENCES

[1] H.J. Böhmer, F.J. Ebert, W. Trojahn, M50NiL bearing material – heat treatment, material properties and performance in comparison with M50 and RBD. Lubr. Eng. **48**, 28-35 (1992).

[2] M. Roy, S. Saha, K. Valleti, Microstructure and Wear of Cathodic Arc Physical Vapor Deposited TiAlN, TiCrN and n-TiAlN/α -Si_3N_4 Films. Defence Science Journal **70**, 6, 656-663 (2020).

[3] H. Song, J. Chen, Z. Liu, N. Jiang, Preparation of a novel multilayered AlSnCu coating for journal Bearings. Surface Engineering **38** (3), 244-251 (2022).

[4] A. Pauschitz, J. Schalko, T. Koch, C. Eisenmenger-Sittner, S. Kvasnica, M. Roy, Nanoindentation and AFM Study of PECVD DLC and Reactively Sputtered Ti Containing Carbon Films. Bulletine of Material Science **26**, 585-591 (2003).

[5] S. Xu, Z. Zhou, Y. Zhou, K. Zhang, Improve adhesion of CrN coatings on TC4 alloy substrates by discharge current modulation in magnetron sputtering. Surface Engineering **39** (6), 761-768 (2023).

[6] Y. Wang, H.T. Liu, H.F. Cheng, Characterisation of CVD carbon coatings on Nextel TM 440 fibres. Surface Engineering **32** (3), 218-222 (2016).

[7] M. Roy, D. Steinmuller-Nethl, A. Tomala, C. Tomastik T. Koch, A. Pauschitz, Tribological Investigation of Nanocrystalline Diamond Film at Low Load under Different Trybosystems. Diamond and Related Materials **20**, 573-583 (2011).

[8] O. Karabechtchikova, S.M. Hsiang, R.D. Sisson, Multi-objective optimisation of gas carburizing process in batch furnaces with endothermic carburizing atmosphere. Surface Engineering **25** (1), 43-49 (2009).

[9] C.S. Zhang, M.F. Yan, Z. Sun, Experimental and theoretical study on interaction between lanthanum and nitrogen during plasma rare earth nitriding Appl. Surf. Sci. **287**, 381-388 (2013).

[10] Y. Li, W. Li, X. Zhu, H. Zhou, X. Jin, Mechanism of improved hydrogen embrittlement resistance of low-temperature plasma carburised stainless steel. Surface Engineering **34** (3), 189-192 (2018).

[11] Z. Sun, C.S. Zhang, M.F. Yan, Microstructure and mechanical properties of M50NiL steel plasma nitrocarburized with and without rare earths addition. Mater. Design **55**, 128-36 (2014).

[12] C.S. Zhang, M.F. Yan, Z. Sun, Y.X. Wang, Y. You, B. Bai, L. Chen, Z. Long, R.W. Li, Optimizing the mechanical properties of M50NiL steel by plasma nitrocarburizing. Appl. Surf. Sci. **315**, 28-35 (2014).

[13] N. Krishnaraj, M. Roy, Tribology of diffusion treated surfaces, in: M. Roy (Ed.), Surface Engineering for Enhanced Performance Against Wear, Printforce, the Netherlands, Springer, Austria 01, 101-147 (2013).

[14] M. Jayalakshmi, Prashant Huilgol, B. Ramachandra Bhat, K. Udaya Bhat, Microstructural characterization of low temperature plasma-nitrided 316L stainless steel surface with prior severe shot peening. Materials and Design **108**, 448-454 (2016).

[15] M.V. Leite, C.A. Figueroa, S. Corujeira Gallo, A.C. Rovani, R.L.O. Basso, P.R. Mei, I.J.R. Baumvol, A. Sinatora, Wear mechanisms and microstructure of pulsed plasma nitrided AISI H13 tool steel. Wear **269**, 466-472 (2010).

[16] M. Naeem, J.C. Díaz-Guillen, Ayesha Khalid, I. Guzman-Flores, R. Munoz-Arroyo, Javed Iqbal, RRM Sous, Improved wear resistance of AISI-1045 steel by hybrid treatment of plasma nitriding and post-oxidation. Tribology International **175**, 107869 (2022).

[17] Bo Wang, Wantang Fu, Fan Dong, Guofeng Jin, Weiwei Feng, Zhenhua Wang, Shuhua Sun, Significant acceleration of nitriding kinetics in pure iron by pressurized gas treatment. Materials and Design **85**, 91-96 (2015).

[18] X.A. Wang, M.F. Yan, C.S. Zhang Y.X. Zhang, B. Bai, L. Chen, Z. Long, R.W. Li, Insights into plasma nitriding behaviour of M50NiL steel with different initial microstructures. Materials Science and Technology **30**, 10, 1248-1253 (2014).

[19] G.-M. Li, Y.-L. Liang, X.-F. Zhang, H. Sun, Y.-G. Cao, Effect of the carburized layer on the plasma nitriding behavior of duplex treated M50NiL steel. Mater. Res. Express **6**, 096550 (2019).

[20] R. Toppo, M. Roy, Influence of Various Counter-bodies on the Sliding Friction and Wear Response of M50 Steel, Ironmaking and Steelmaking: Processes, Products and Applications, Ironmaking & Steelmaking Processes. Products and Applications **50**, 5, X, 470-484 (2022).

[21] S.D. Jacobsen, R. Hinrichs, C. Aguzzoli, C.A. Figueroa, I.J.R. Baumvol, M.A.Z. Vasconcellos, Influence of current density on phase formation and tribological behavior of plasma nitrided AISI H13 steel. Surface & Coatings Technology **286**, 129-139 (2016).

[22] J. Yao, F. Yan, Y. Yang, M. Yan, Y. Zhang, Comprehensive analysis of nitriding behavior and synergistic strengthening mechanism on quenched M50 steel. Surface & Coatings Technology **436**, 128307 (2022).

[23] S.D. Jacobsen, R. Hinrichs, I.J.R. Baumvol, G. Castellano, M.A.Z. Vasconcellos, Depth distribution of martensite in plasma nitrided AISI H13 steel and its correlation to hardness. Surface & CoatingsTechnology **270**, 266-271 (2015).

[24] B. Wang, X. Zhao, W. Li, M. Qin, J. Gu, Effect of nitrided-layer microstructure control on wear behavior of AISI H13 hot work die steel. Appl. Surf. Sci. **431**, 39-43 (2018).

[25] Y. Duan, S. Qu, S. Jia, X. Li, Evolution of wear damage in gross sliding fretting of a nitrided high-carbon high-chromium steel. Wear **464-465**, 203548 (2021).

[26] E. Balikci, O. Yaman, Investigation of liquid bath nitriding of selected steels. Surface Engineering **27** (8), 609-615 (2011).

[27] P.C. Van Wiggen, H.C.F. Rozendaal, E.J. Mittemeijer, The nitriding behaviour of iron-chromium-carbon alloys. J. Mater. Sci. **20**, 4561-4582 (1985).

[28] C. Ruset, S. Ciuca, E. Grigore, The influence of the sputtering process on the constitution of the compound layers obtained by plasma nitriding. Surf. Coating. Technol. **174**, 1201-1205 (2003).

[29] Z.-B. Cai, X.-D. Chen, T. Rui, L.-W. Wang, X.-H. Liu, F. Zhang, Investigation of the fretting corrosion mechanism of QPQ-treated TP316H steel in liquid sodium at 450°C, Corrosion Sci. **201**, 110282 (2022).

[30] L.D. Tadepalli, A.M. Gosala, L. Kondamuru, S.C. Bairi, R. Subbiah, S.K. Singh, A review on effects of nitriding of AISI409 ferritic stainless steel. Mater. Today. Pro. **26**, 1014-1020 (2022).

[31] R. Huang, J. Wang, S. Zhong, M. Li, J. Xiong, H. Fan, Surface modification of 2205 duplex stainless steel by low temperature salt bath nitrocarburizing at 430°C. Appl. Surf. Sci. **271**, 93-97 (2013).

[32] H. Dong, S-phase surface engineering of Fe-Cr, Co-Cr and Ni-Cr alloys. Int. Mater. Rev. **55**, 2, 65 (2010).

[33] J. Wang, Y. Lin, J. Yan, D. Zen, Q. Zhang, R. Huang, H. Fan, Influence of time on the microstructure of AISI 321 austenitic stainless steel in salt bath nitriding. Surface & Coatings Technology **206**, 3399-3404 (2012).

[34] G.J. Li, Q. Peng, C. Li, Y. Wang, J. Gao, S.-Y. Chen, J. Wang, B.-L. Shen, Microstructure analysis of 304L austenitic stainless steel by QPQ complex salt bath treatment. Mater. Charact. **59** (9), 1359-1363 (2008).

[35] Xi. Zhang, J. Wang, H. Fan, D. Pan, Erosion–corrosion resistance properties of 316L austenitic stainless steels after low-temperature liquid nitriding. Appl. Surf. Sci. **440**, 755-762 (2018).

[36] M.T. Umemura, L.B. Varela, C.E. Pinedo, R.C. Cozza, A.P. Tschiptschin, Assessment of tribological properties of plasma nitrided 410S ferritic-martensitic stainless steels. Wear **426-427**, 49-58 (2019).

[37] M.D. Conci, A.C. Bozzi, A. Ri. Franco, Effect of plasma nitriding potential on tribological behaviour of AISI D2 cold-worked tool steel. Wear **317** (1-2), 188-193 (2014).

[38] S.K. Kim, J.S. Yoo, J.M. Priest, M.P. Fewell, Characteristics of martensitic stainless steel nitrided in a low-pressure RF plasma. Surf. Coat. Technol. 163-164, 380-385 (2003).

[39] L.F. Zagonel, R.L.O. Basso, F. Alvarez, Precipitates Temperature Dependence in Ion Beam Nitrited AISI H13 Tool Steel. Plasma Process. Polym. **4**, S736-S740 (2007).

[40] A. Berrais, A. Boudebane, M. Labaiz, A. Montagne, S. Lemboub, M.Z. Touhami, A. Ourdjini, Analysis of wear of a nitrided AISI H13 hot work tool steel in an aluminium hot extrusion process. Wear **514-515**, 204587 (2023).

[41] C. Zheng, Y. Liu, H. Wang, H. Zhu, R. Ji, Z. Liu, Y. Shen, Research on the effect of gas nitriding treatment on the wear resistance of ball seat used in multistage fracturing. Materials and Design **70**, 45-52 (2015).

[42] Y. Duan, S. Qu, S. Jia, X. Li, Evolution of wear damage in gross sliding fretting of a nitrided high-carbon high-chromium steel. Wear **464-465**, 203548 (2021).

[43] G. Castro, A. Fernandez-Vicente, J. Cid, Influence of the nitriding time in the wear behaviour of an AISI H13 steel during a crankshaft forging process. Wear **263**, 1375-1385 (2007).

[44] A.P. Murali, M. Alphonse, D. Ganesan, S. Salunkhe, H.M.A.M. Hussein, Sliding wear behaviour of salt bath nitrided 316LN austenitic stainless steel. Applied Surface Science Advances **15**, 100401 (2023).

[45] T. Peng, M. Daia, W. Caia, W. Wei, K. Wei, J. Hu, The enhancement effect of salt bath preoxidation on salt bath nitriding for AISI 1045 steel. Applied Surface Science **484**, 610-615 (2019).

[46] T.-S. Shih, Y.-S. Huang, C.-F. Chen, Constituted oxides/nitrides on nitriding 304, 430 and 17-4 PH stainless steel in salt baths over the temperature range 723 to 923K. Applied Surface Science **258**, 81-88 (2011).

[47] J. Valdés, J. Solis, R. Mercado, J. Oseguera, H. Carreon, C. Aguilar, A. Medina, Influence of plasma nitriding treatment on the microscale abrasive wear behavior of AISI 4140 steel. Materials Letters **324**, 132629 (2022).

[48] D. Chen, M. Liu, X. Liu, Y. Zhou, X. Wang, Y. Zhou, Oxidation behavior of 304 stainless steel with modified layer by plasma nitriding in High temperature and pressurized Water. Corrosion Science **186**, 109486 (2021).

[49] Y. Yang, X. Zhou, X.Z. Dai, J. Li, S.H. Zhang, C.S. Zhang, J.C. Ding, Jun Zheng, Comparative study of plasma nitriding and plasma oxynitriding for optimal wear and corrosion resistance: Influences of gas composition. Journal of Materials Research and Technology **15**, 448-459 (2021).

[50] L.F. Zagonel, C.A. Figueroa, R. Droppa Jr., F. Alvarez, Influence of the process temperature on the steel microstructure and hardening in pulsed plasma nitriding. Surface & Coatings Technology **201**, 452-457 (2006).

[51] S.M.Y. Soleimani, A.R. Mashreghi, S.S. Ghasemi, M. Moshrefifar, The effect of plasma nitriding on the fatigue behavior of DIN 1.2210 cold work tool steel. Materials and Design **35**, 87-92 (2012).

[52] F.A.P. Fernandes, S.C. Heck, C.A. Picone, L.C. Casteletti, On the wear and corrosion of plasma nitrided AISI H13. Surface & Coatings Technology **381**, 125216 (2020).

[53] M.B. Karamış, K. Yıldızlı, G. Carkıt Aydın, Sliding/rolling wear performance of plasma nitrided H11 hot working steel. Tribology International **51**, 18-24 (2012).

[54] M.D. Manfrinato, L.S. de Almeida, L.S. Rossino, A.M. Kliauga, L. Melo-Maximo, D.V. Melo-Maximo, R.C. Moron, Scratch testing of plasma nitrided and nitrocarburized AISI 321 steel:

Influence of the treatment temperature. Materials Letters **317**, 132083 (2022).

[55] C.V. Funch, T.L. Christiansen, M.A.J. Somers, Gaseous nitriding of additively manufactured maraging steel; nitriding kinetics and microstructure evolution. Surface & Coatings Technology **432**, 128055 (2022).

[56] M. Godec, F. Ruiz-Zepeda, B. Podgornik, C. Donik, A. Kocijan, D.A. Skobir Balantic, The influence of the plasma-nitriding temperature on the microstructure evolution and surface properties of additive-manufactured 18Ni300 maraging steel. Surface & Coatings Technology **433**, 1280089 (2022).

[57] G. Luoa, Z. Zheng, L. Ning, Z. Tan, J. Tong, E. Liu, Failure analysis of AISI 316L ball valves by salt bath nitriding. Engineering Failure Analysis **111**, 104455 (2020).

[58] N. Krishnaraj, P. Bala Srinivasan, K.J.L. Iyer, S. Sundaresan, Optimization of compound layer thickness for wear resistance of nitrocarburized H11 steels. Wear **215**, 123-130 (1998).

[59] S.C. Lim, M.F. Ashby, Wear-Mechanism maps. Acta. Metal. **35**, 24, 5, 805-810 (1987).

[60] M. Roy, A. Pauschitz, J. Wernisch, F. Franek, Influence of Mating Surface on Elevated Temperature Wear of 253 MA Alloy. Materials and Corrosion **55**, 259-273 (2004).

[61] M. Roy, A. Pauschitz, F. Franek, Elevated Temperature Wear of 253 MA Alloy. In Proc. 3rd AIMETA International Tribology Conference, Vietri sul Mare, Italy, 18th-20th September 2002, p. 259.